JVST A
Journal of Vacuum Science & Technology A

Review of recent studies on nanoscale electrical junctions and contacts: Quantum tunneling, current crowding, and interface engineering

Cite as: J. Vac. Sci. Technol. A **40**, 030802 (2022); https://doi.org/10.1116/6.0001724
Submitted: 28 December 2021 • Accepted: 13 April 2022 • Published Online: 05 May 2022

Sneha Banerjee and Peng Zhang

COLLECTIONS

Note: This paper is a part of the Special Topic Collection: Celebrating the Early Career Professionals Contributing to the Advancement of Thin Films, Surfaces, Interfaces, and Plasmas.

This paper was selected as Featured

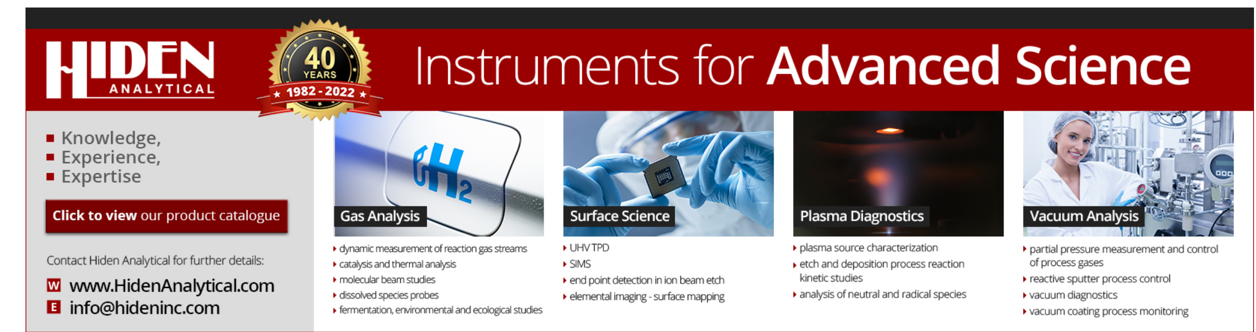

© 2022 Author(s).

REVIEW
avs.scitation.org/journal/jva

Review of recent studies on nanoscale electrical junctions and contacts: Quantum tunneling, current crowding, and interface engineering

Cite as: J. Vac. Sci. Technol. A **40**, 030802 (2022); doi: 10.1116/6.0001724
Submitted: 28 December 2021 · Accepted: 13 April 2022 ·
Published Online: 5 May 2022

Sneha Banerjee[a),b)] and Peng Zhang[c)]

AFFILIATIONS

Department of Electrical and Computer Engineering, Michigan State University, East Lansing, Michigan 48824

Note: This paper is a part of the Special Topic Collection: Celebrating the Early Career Professionals Contributing to the Advancement of Thin Films, Surfaces, Interfaces, and Plasmas.
[a)]snebane@sandia.gov
[b)]**Present address:** Electrical Models and Simulation, Sandia National Labs, Albuquerque, New Mexico 87123.
[c)]**Author to whom correspondence should be addressed:** pz@egr.msu.edu

ABSTRACT

The study of charge carrier transport at nanoscale electrical contacts is crucial for the development of next-generation electronics. This paper reviews recent modeling efforts on quantum tunneling, current crowding, and contact resistance across electrical interfaces with nanometer scale dimensions. A generalized self-consistent model for quantum tunneling induced electron transport in metal–insulator–metal (MIM) junctions is summarized. Rectification of a dissimilar MIM junction is reviewed. A modified two-dimensional (2D) transmission line model is used to investigate the effects of spatially varying specific contact resistivity along the contact length. The model is applied to various types of electrical contacts, including ohmic contacts, MIM junction based tunneling contacts, and 2D-material-based Schottky contacts. Roughness engineering is recently proposed to offer a possible paradigm for reducing the contact resistance of 2D-material-based electrical contacts. Contact interface engineering, which can mitigate current crowding near electrical contacts by spatially designing the interface layer thickness or properties, without requiring an additional material or component, is briefly reviewed. Tunneling engineering is suggested to eliminate severe current crowding in highly conductive ohmic contacts by introducing a thin tunneling layer or gap between the contact members. Unsolved problems and challenges are also discussed.

Published under an exclusive license by the AVS. https://doi.org/10.1116/6.0001724

I. INTRODUCTION

In modern electronics, nanoscale electrical junctions are ubiquitous; they are naturally formed in transistors,[1,2] scanning tunneling microscopes,[3,4] thin film contacts,[5–9] and two-dimensional (2D) material, nanowire, nanofiber, or nanorod based novel devices.[10–17] Based on the materials of the contact members and the interfacial layers, these junctions can be of ohmic, Schottky, or tunneling type. This review paper collates recent theoretical studies on the current transport in nanoscale electrical junctions and electrical contacts.[18]

Tunneling type contacts are especially common where the contacting members are separated by very thin insulating layers.[19–21] When two conductors are separated by a sufficiently thin (in nanometer or sub-nanometer scale) insulator, electrical current can flow between them by quantum tunneling. As the tunneling induced stray currents in the circuit can cause device malfunction, this phenomenon imposes some serious challenges to the modern electronics industry where electrodes in the nanometer scale are common.[1,2,22,23] However, in recent times, quantum tunneling has been utilized to develop novel devices that offer advantages over the shortcomings of down scaling. Next-generation transistors that are expected to further extend Moore's law, such as tunnel field effect transistors (TFETs),[24,25] single electron transistors (SETs),[26–29] and graphene-based field effect transistors, rely on quantum tunneling for their operation. Tunneling electron emission through vacuum nanogap is also common in miniaturized vacuum and plasma electronic devices[30–38] and plasmonic nanogaps.[39] Recent technologies also attempt to combine the advantages of ballistic transport through

Published under an exclusive license by the AVS

vacuum with scalability, reliability, and low cost of silicon technology.[30,40,41] Nanoscale devices based on quantum tunneling principles are expected to become increasingly important in future electronics industry. To enable the practical use of such devices, a comprehensive understanding of the quantum current transport is necessary.

On the other hand, tunneling resistivity is one of the major obstacles for the development of low-dimensional material-based devices. Transistors based on nanotubes, nanofibers, and 2D materials use arrays or networks of nanostructures as their channel material.[15–17,20,42–45] The overall transistor performance is critically dependent upon the tunneling resistivity between these nanostructures.[20,42–44] To realize the excellent electrical properties of novel low-dimensional materials on the circuit level and to develop scalable electronics based on them, contact engineering is crucial.[46]

Current flow in an electrical circuit is usually nonhomogeneous. Localized increase of current density or the current crowding effect[5,6,9,47–50] is a serious and persistent problem in the electronics industry. Current crowds near a bend or a constriction, and it is especially strong at the vicinity of contact edges.[8,50–54] Current crowding leads to nonuniform heat generation in the contact area. The excessive amount of Joule heating deposited at the contact region because of the large contact resistance is another critical concern of very-large-scale-integrated (VLSI) circuit engineers.[55–57] The individual or combined effects of current crowding, contact resistance, and nonuniform Joule heating are responsible for about 40% of all electrical/electronics failure, ranging from small scale modern consumer electronics, such as hand-held or wearable devices, personal computers, to large-scale space vehicles, particle accelerators, nuclear facilities, and military systems.[30,54,58–64]

Contact problems have become more prominent nowadays because of the growing demands for advanced computation, high speed, low cost, high packing density, and low power consumption. In densely packed integrated circuits (ICs), current crowding, contact resistance, and poor heat dissipation options cause thermomigration and thermal cross talk, aggravation of electromigration, and in the worst scenario, lead to thermal runaway and catastrophic burn-out type failure.[61] Current crowding also causes localized overheating and formation of hotspots, leading to component breakdown.[61,65] In advanced 2D-material-based electronic devices, forming good electrical contacts is a major concern. 2D materials, such as molybdenum disulfide (MoS_2), black phosphorus, boron nitride, graphene have been demonstrated to be excellent channel materials for ultrathin field-effect transistors.[2,34,65,66] However, the current crowding effect and the unusually high contact resistance at the 3D metal and the 2D semiconductor interfaces[65–68] hinder the development of such electronics. In modern compact high power microwave sources and pulsed power systems, poor electrical contact prevents efficient power coupling to the load,[62] produces unwanted plasma,[69] and in the worst-case scenario, damages the electrodes and circuits. Therefore, a comprehensive and systematic study of the current transport and electrical contacts in nanoscale electrical junctions is essential to further advance modern electronics.

In this paper, we review recent studies conducted at the Michigan State University on the modeling of nanoscale electrical junctions and electrical contacts.[18] We start with a mini historical review of theoretical and modeling studies on quantum tunneling in metal–insulator–metal (MIM) junctions, and current flow distribution and contact resistance in electrical contact structures (Sec. II). We would like to point out that it is not our intention to give a comprehensive review of the topics; rather, to provide essential background information for the later discussion. Next, we present the modeling of quantum tunneling in MIM nanojunctions (Sec. III). Modeling of tunneling electrical contacts and 2D-material-based Schottky contacts using modified transmission line models (TLMs) is presented in Secs. IV and V, respectively. In Sec. VI, we discuss the recently proposed interface engineering methods to reduce current crowding effects. Finally, we conclude the paper by noting a few aspects of future research in Sec. VII.

II. MINI HISTORICAL REVIEW

A. Quantum tunneling in metal–insulator–metal junctions

The work on quantum tunneling started as early as 1926, when Schrödinger published his landmark equation for wave function in quantum mechanics.[70] The same year, Wenzel, Kramers, and Brillouin developed a semiclassical method—known as the Wenzel–Kramers–Brillouin (WKB) method for finding approximations to the one-dimensional time-independent Schrödinger equation.[71,72] This WKB method is widely used to calculate transmission and reflection coefficients through a smooth and slowly varying potential barrier. In 1933, Sommerfeld and Bethe published a theoretical study of tunneling in MIM junctions for very low and high voltages using the WKB approximation.[73] In 1935, Holm extended the theory to include intermediate voltages.[74] The challenge for this kind of study was to determine the actual shape of the potential barrier in the vacuum gap or insulator. In 1963, Simmons closely modeled the shape of the barrier and improved its accuracy.[19]

Tunneling effects between electrodes separated by thin insulating films have been studied extensively by Simmons[19,75] in 1960s. His formulas have since been widely used for evaluating tunneling current in MIM junctions. The tunneling current in Al-Al_2O_3-Al structures has been experimentally studied and evaluated using Simmons' theory.[76] Although widely used, Simmons' theory has some limitations: (1) the formulas are derived by considering only the emission process from the electrodes, where the effects of image charge are considered, but the electron space-charge potential and the electron exchange-correlation potential inside the insulator thin films are ignored; (2) this model is reliable only in the low voltage regime for limited parameter space;[21] (3) it fails to predict the maximum possible tunneling current in an MIM junction.

There are several theoretical[77–79] and experimental[80,81] studies on space-charge effects in a vacuum nanogap. The Child–Langmuir (CL) law gives the space-charge-limited (SCL) current in a plane-parallel vacuum diode. This classical value for the limiting current can be exceeded by a large factor in nanoscale vacuum gap because of tunneling. The new limit is referred as the quantum CL (QCL) law.[77,78] The effects of exchange-correlation potential in a vacuum nanogap have also been studied systematically.[82]

In 2015, a general scaling law for the quantum tunneling current in nano- and sub-nanoscale MIM junctions has been

Published under an exclusive license by the AVS

developed by self-consistently solving the coupled Schrödinger and Poisson equations.[21] Zhang's model[21] was formulated for similar electrodes. It includes the effects of space-charge and exchange-correlation potential, as well as current emission from both electrodes. The current–voltage (J–V) characteristics has three distinct regimes: (1) the direct tunneling regime, where it follows Simmons's formula,[19] (2) field emission regime, where it becomes close to the Fowler-Nordheim law,[83] and (3) SCL regime, where it approaches the quantum Child-Langmuir law.[77,78] The recent extension of Zhang's work to include the effects of dissimilar metal electrodes[84] will be presented in Sec. III.

B. Current flow distribution and contact resistance

Different theoretical models have been developed over time to characterize micro- and nano-scale thin film-based contacts, including conformal mapping, transmission line model (TLM), field theory, and numerically solving Laplace's equation in the contact area.[9,30,47,60,85–88] In this paper, we briefly review the TLM, which is in plenty of variant or extended forms, has been widely used for analyzing metal–semiconductor planar contacts, due to its simplicity.

In 1969, Murrmann and Widmann[49] used a simple steady state TLM to characterize planar metal–semiconductor contacts and defined important contact characterization parameters, such as, contact resistance R_c (in Ω), semiconductor sheet resistance beneath the contact R_{sh} (in "ohm per square," denoted by Ω/□), and specific contact resistivity ρ_c (in Ω/cm^2). In 1972, Berger[89] provided a thorough characterization of contact resistance and contact resistivity and defined the current *transfer length* L_T, over which most of current transfer takes place from semiconductors to metals, indicating strong current crowding. In 1980, Reeves extended the formulation for Cartesian contacts to circular contact structures.[90] In 1995, Reeves and Harrison[91] further extended the theory to alloyed ohmic contacts using a trilayer transmission line model (TTLM).[91–93]

Although the TLM theory is one of the most commonly used models to characterize planar contacts, allowing important contact parameters (ρ_c, R_{sh}, R_c) to be extracted or calculated, it has several known limitations: (1) the sheet thickness of the contact material is assumed to be zero, forcing current flow to be one-dimensional, (2) it is applicable only for ohmic contacts or contacts that can be approximated as ohmic, (3) specific contact resistivity is assumed to be constant along the contact length. Various modifications of this theory have been attempted to overcome some of the limitations.

The "zero sheet thickness" restriction was relaxed by Berger[89] in his extended transmission line model (ETLM) with current still restricted to one-dimensional flow, by adding a virtual specific contact resistivity of 0.19 $\rho_2 h_2$, where ρ_2 is the resistivity and h_2 is the thickness of the semiconductor layer. This ETLM has been widely used in the literature.[94,95] In 2014, Zhang and Lau[94] compared the TLM, ETLM with an exact field solution. They found that TLM can be used to accurately evaluate contact resistance if $\eta = \rho_c/\rho_2 h_2 > 2$, which is typically the case for electrical contacts and junctions between thin films, nanotubes, and nanorods, since the height of the contact members is in a nanometer scale. Indeed, TLM has been used to model and measure various low-dimensional material-based contacts, such as, metal-CNT,[96] metal-nanofibers, gold-MoS_2,[66,97,98] indium-MoS_2,[66] nickel-MoS_2,[98] and graphene-metal ohmic contacts.[99]

The figure of merit used for contact characterization is the specific contact resistivity ρ_c, defined as the ratio of the voltage drop V_c to current density J_c across the contact. It has a constant value for ohmic contacts. If the junction is highly nonlinear, the ohmic approximation fails to give accurate characterization of the contact. In 2011, Piotrzkowski *et al.*[100] generalized TLM to include functional dependence of $J_c(V_c)$. In 2014, He *et al.*[101] proposed a numerical method to characterize nonlinear metal–semiconductor contacts by adding a Schottky diode to the standard TLM in series with the original pure resistance to account for the nonlinearity.

Another key limitation of the standard TLM is its constant ρ_c assumption along the entire contact length, treating the junction one-dimensional. This treatment is valid only for ohmic contacts with uniform interfacial layer properties. In practical contacts, ρ_c depends on local voltage drop and local contact current density, and therefore, are expected to vary spatially. Physically, this spatial dependence of ρ_c may be introduced by a variety of factors, such as, the inherent nonlinearity of the current density–voltage ($J - V$) profiles of tunneling and Schottky junctions, rough interfacial layer, nonuniform distribution of oxides, contaminants or impurities in the contact layer, etc. In this paper, we will review the recently developed modified 2D TLM that includes the effects of spatially varying ρ_c along the contact length.[102–105]

The 2D-TLM[102,103] was applied for ohmic contacts. TLM coupled with the thermionic injection model[104,106] was used for Schottky contacts (see Sec. V), and coupled with the self-consistent quantum model[21,84] for tunneling type contacts (see Sec. IV). A method to control current distribution was demonstrated, by engineering the interface layer properties and geometry[107] (see Sec. VI). It was found that current crowding can be mitigated by strategically designing the specific contact resistivity ρ_c along the contact length.

III. QUANTUM TUNNELING IN DISSIMILAR METAL–INSULATOR–METAL JUNCTIONS

A generalized self-consistent model for quantum tunneling current in dissimilar metal–insulator–metal junction is developed, by solving the coupled Schrödinger and Poisson equations.[84] When two electrodes with different work functions are brought together to form a dissimilar MIM junction, the tunneling current depends on the polarity of the external bias voltage.[75] This asymmetry of the $J - V$ characteristic is crucial to several applications, such as scanning tunneling microscopes, harmonic mixers, rectifiers, millimeter wave and infrared detectors.[108] In recent years, several efforts have been made to enhance this asymmetry.[108–110] Dissimilar MIM junctions are also common in nanoscale electrical contacts.[102]

A typical dissimilar MIM tunneling junction with different bias conditions is shown in Fig. 1. Following Simmons,[75] forward bias (FB) and reverse bias (RB) of the MIM junction were defined

Published under an exclusive license by the AVS

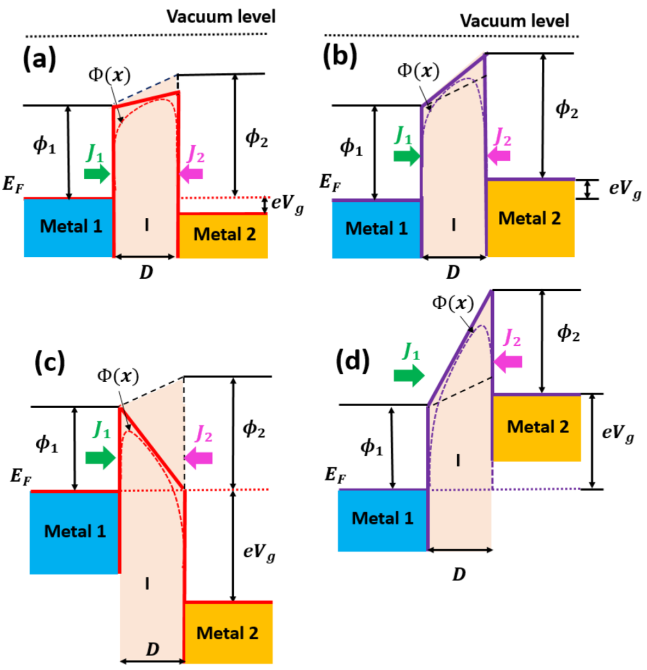

FIG. 1. Dissimilar MIM tunneling junction. The metal electrodes have equilibrium Fermi level E_F and work function W_1 and W_2 (in these schematics, $W_2 > W_1$). $\phi_1 = W_1 - X$, $\phi_2 = W_2 - X$, where X is the electron affinity of the insulator. The insulator thin film thickness is D. The applied voltage bias is V_g. The current densities emitted from the electrode 1 and 2 into the gap are J_1 and J_2, respectively. (a) and (c) reverse bias condition (metal 2 is positively biased); (b) and (d) forward bias condition (metal 2 is negatively biased). (a) and (b) represent low and (c) and (d) represent high bias voltage conditions. Reprinted with permission from Banerjee and Zhang, AIP Adv. **9**, 085302 (2019). Copyright 2019 AIP Publishing LLC.

when the metal electrode with a higher work function is negatively and positively biased, respectively. The asymmetry of $J - V$ characteristics in forward and reverse bias and its dependence on various material properties and input voltages were studied comprehensively.[84]

The potential barrier in the insulator layer (Fig. 1) (Ref. 84) is $\Phi(x) = E_F + \Phi_w(x) + \Phi_{image}(x) + eV(x) + \Phi_{xc}(x)$, where E_F is the equilibrium Fermi level; $\Phi_w(x) = \phi_1 + (\phi_2 - \phi_1)x/D$;[75] $\phi_1 = W_1 - X$, $\phi_2 = W_2 - X$; W_1 and W_2 are the work functions of metal electrodes 1 and 2, respectively, X is the electron affinity of the insulator. $\Phi_{image}(x)$ is the image charge potential;[111] $\Phi_{xc}(x)$ is the exchange-correlation potential calculated by the Kohn–Sham local density approximation (LDA);[112] and $eV(x)$ includes space-charge potential and the external bias voltage. The space-charge potential is calculated by solving the coupled Schrödinger and Poisson equations.[21] The boundary conditions are derived from the applied bias, charge conservation along x, and the continuity of the wave function and its derivative at $x = 0$ and $x = D$.

The net tunneling current density (J_{net}) is the superposition of the current emitted from both electrodes ($J_{1,2}$). $J_{1,2}$ depends on the tunneling probability and electron supply function from the electrodes. In this work,[21,84] the electron supply function at the two electrodes is calculated from the free-electron theory of metal,[113] and the tunneling probability of electrons through the barrier $\Phi(x)$ is calculated from the WKB approximation.[114]

It was found that, in the direct tunneling regime, the FB current exceeds slightly, as shown in Fig. 2(a). At high voltages in the field emission regime, the FB and RB characteristics cross over. This crossover behavior is important and occurs because the tilt of the potential barrier changes its direction for the RB condition in the high voltage region [cf. Figs. 1(a) and 1(c)]. For higher voltages, the electrons tunnel through a lower effective potential barrier height in RB condition than that in the FB condition, and the $J - V$ characteristics become significantly asymmetric [Fig. 2(a)]. The asymmetry between FB and RB currents in the field emission regime increases significantly as the work function difference between the two metal electrodes $|\Delta W|$ increases. The asymmetry disappears when the gap width D is small and it increases significantly when D is increased [Fig. 2(b)]. For fixed work functions, the FB and RB characteristics tend to crossover at about the same voltage [Fig. 2(b)], which is insensitive to the D values.[84] In the space-charge-limited regime, the cathode current and therefore net current J_{net} approaches the maximum tunneling current density across a nanogap for a given V_g and D, i.e., the quantum Child–Langmuir law.[77,78]

Since the electron tunneling time through a barrier of nm-scale thickness is usually less than 1 fs,[115–119] this self-consistent model[84] can be applied to nanojunctions operating up to the near infrared frequency, enabling studies on the effects of tunneling resistance in various nanoscale electrical structures with time-varying bias, such as tunneling plasmonic resonator arrays, THz induced scanning tunneling microscopes (THz-STMs), etc.

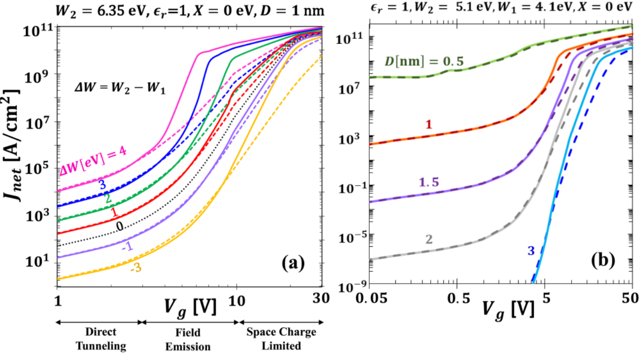

FIG. 2. (a) Effects of work function difference $\Delta W = W_2 - W_1$ on the $J - V$ characteristics of a dissimilar MIM junction with $D = 1$ nm vacuum gap ($\epsilon_r = 1$, $X = 0$ eV). Lines from top to bottom, $\Delta W = 4$ eV, 3 eV, 2 eV, 1 eV, 0 eV, −1 eV, −3 eV. The work function of metal 2 is kept fixed, $W_2 = 6.35$ eV (Pt). (b) The effects of gap width (D) on the $J - V$ characteristics of a dissimilar MIM junction with vacuum gap. Lines from top to bottom, $D = 0.5$ nm, 1 nm, 1.5 nm, 2 nm, 3 nm. Solid and dashed lines represent RB and FB conditions, respectively. Reprinted with permission from Banerjee and Zhang AIP Adv. **9**, 085302 (2019). Copyright 2019 AIP Publishing LLC.

Published under an exclusive license by the AVS

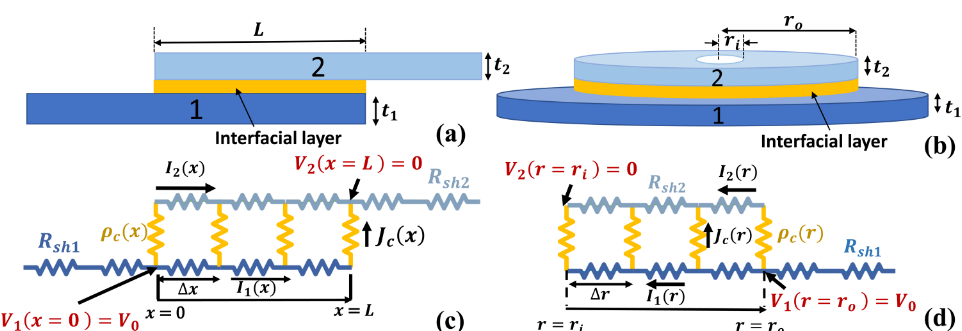

FIG. 3. Electrical contact between two contacting members in (a) Cartesian, (b) circular geometry. (c) and (d) its corresponding transmission line model. In (a) and (b), a thin interface layer (ohmic, Schottky, or tunneling type) is sandwiched between the two contacting members. The thicknesses of thin film 1 and 2 are t_1 and t_2, respectively. Reprinted with permission from Banerjee *et al.*, Phys. Rev. Appl. **15**, 064048 (2021). Copyright 2021 American Physical Society.

IV. TUNNELING ELECTRICAL CONTACTS

A 2D-TLM that includes the effects of spatially varying specific contact resistivity (Fig. 3) was proposed in Ref. 107. For tunneling junctions, because of the nonlinear current–voltage characteristics (Fig. 2),[19,21,75,84] the specific resistivity becomes spatially dependent, even for an insulating layer with uniform thickness. Therefore, the state-of-the-art methods that treat those junctions as one-dimensional,[20] become unreliable.

The governing equations are derived from Kirchoff's laws for current and voltage. For Cartesian electrical contacts in Fig. 3(a), its TLM in Fig. 3(c) gives the following four equations,[102] $\partial I_1(x)/\partial x = -wJ_c(x)$, $\partial V_1(x)/\partial x = -I_1(x)R_{sh1}/w$, $\partial I_2(x)/\partial x = wJ_c(x)$, $\partial V_2(x)/\partial x = -I_2(x)R_{sh2}/w$, where $I_{1,2}(x)$ represents the current flowing at x through the lower or upper contact member, respectively, $V_{1,2}(x)$ is the local voltage at x along the lower or upper contact member, respectively, and w is the effective transverse dimension of the contacts. $J_c(x) = V_g(x)/\rho_c(x)$ and $V_g(x) = V_1(x) - V_2(x)$ are the local current density and the local voltage drop across the contact interface at x, respectively. Note that $I_1(x) + I_2(x) = I_{tot} =$ constant, where I_{tot} is the total current in the circuit, to be determined from the boundary conditions, $V_1(x = 0) = V_o$, $I_2(x = 0) = 0$, $I_1(x = L) = 0$, $V_2(x = L) = 0$, where V_0 is the externally applied bias voltage. For the contact model in Fig. 3(c), the contact resistance is defined as $R_c = [V_1(0) - V_2(L)]/I_{tot} = V_o/I_{tot}$. Similar formulations were derived for circular (ring) electrical contacts shown in Fig. 3(b) as well.[90,103] Here, the contact resistance is defined as $R_c = [V_1(r_o) - V_2(r_i)]/I_{tot} = V_o/I_{tot}$, where r_o is the outer radius of thin film 2 and r_i is the inner radius of both the films.

Simple analytical solutions were derived for the special case of uniform ρ_c. Figure 4 shows analytical solutions for a Cartesian parallel electrical contact for different normalized specific contact resistivity ($\overline{\rho_c} = \rho_c/R_{sh1}L^2$) and sheet resistance ratio ($\overline{R_{sh2}} = R_{sh2}/R_{sh1}$). For similar contact members [$R_{sh2} = R_{sh1}$ in Fig. 4(a)], current profiles are symmetric, current crowds at the two edges, and this current crowding decreases when ρ_c increases. For dissimilar contact members [$R_{sh2} \neq R_{sh1}$ in Fig. 4(b)], the current profiles are asymmetric. $\overline{R_{sh2}}$ influences the spatial distribution of the current more strongly. The contact resistance increases with both $\overline{\rho_c}$ and $\overline{R_{sh2}}$ [Fig. 4(c)], and it depends more strongly on the specific contact resistivity of the interfacial layer $\overline{\rho_c}$ than on the sheet resistance ratio of the contact members.

Self-consistent numerical solutions were obtained for spatially (or radially) varying ρ_c. For MIM tunneling type contacts, $J_c(x)$ or $J_c(r)$, (Fig. 3) was calculated from the 1D MIM quantum tunneling model at location x or r (Sec. III).[21,84] $\rho_c(x)$ and $\rho_c(r)$ were determined from these contact current densities by $\rho_c = V_g/J_c$. The coupled equations of the TLM and MIM quantum tunneling model were then solved self-consistently.[102,103] The spatial distributions of currents and voltages across such contacts and the total contact resistance[18,102,103] were comprehensively studied for various contact geometry and material properties.

Figure 5 shows the contact current density profiles and the voltage-dependent contact resistance profiles for an annular Cu–vacuum–Cu junction. It was found that the analytical solutions (constant ρ_c assumption along the contact) become unreliable when $\beta = r_i/r_o$ is small, contact length, or input bias voltage is large, or insulating layer thickness D is small.[102,103] For circular contacts, the current density profiles are asymmetric at the two edges even for similar contact members, and this asymmetry decreases as β increases [Fig. 5(a)]. Solving TLM equations

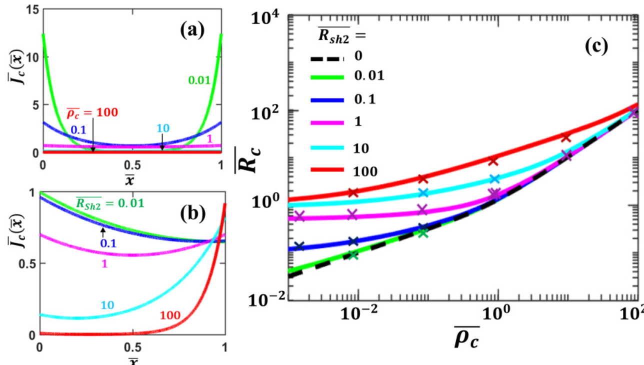

FIG. 4. Analytical solution of Cartesian parallel electrical contact for the special case of uniform specific contact resistivity along contact length L. Normalized contact current density ($\overline{J_c} = J_cR_{sh1}L^2/V_0$) along normalized contact length ($\bar{x} = x/L$) for different (a) normalized specific contact resistivity $\bar{\rho}_c = \rho_c/R_{sh1}L^2$, and (b) sheet resistance ratio of the two contact members $\overline{R_{sh2}} = R_{sh2}/R_{sh1}$. In (a) $\overline{R_{sh2}} = 1$, and in (b) $\overline{\rho_c} = 1$. (c) Normalized contact resistance $\overline{R_c}$ of a parallel contact as a function of $\bar{\rho}_c$. In (c), the dashed line is for the limiting case of $\overline{R_{sh2}} \to 0$ and the cross symbols are from COMSOL 2D simulations. Adapted with permission from Banerjee *et al.*, Sci. Rep. **9**, 14484 (2019). Copyright 2019 Nature; licensed under a Creative Commons Attribution (CC BY) license.

Published under an exclusive license by the AVS

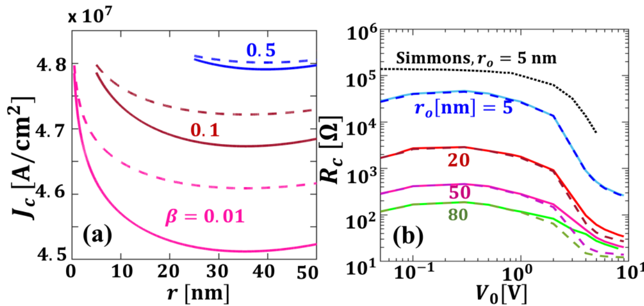

FIG. 5. (a) Tunneling current density across the circular Cu–vacuum–Cu contact interface $J_c(r)$ for different inner radius to outer radius ratio β, with fixed $r_0 = 50$ nm, $V_0 = 1$V and $D = 0.6$ nm. (b) The total contact resistance R_c as a function of input voltage V_0 for different outer radius r_0, with fixed $\beta = 0.01$ and $D = 0.6$ nm. Solid lines are for self-consistent numerical calculations coupling TLM equations and the MIM quantum tunneling formulation (Sec. III). Dashed lines are for analytical calculations with ρ_c calculated using $V_g = V_0$ in the MIM quantum analysis. The dotted line in (b) is for calculations using Simmons equation for tunneling. Reprinted with permission from Banerjee *et al.*, J. Phys. D: Appl. Phys. **53**, 355301 (2020). Copyright 2020 IOP Publishing.

coupling with the Simmons equation [black dotted line in Fig. 5(b)] overestimates contact resistance, and using the MIM tunneling model in Sec. III may give more accurate estimation of the results. For low voltages, the tunneling junction can be represented by the Ohmic approximation since R_c varies little with V_0 in this regime [Fig. 5(b)]. However, as V_0 becomes close or larger than 1 V, R_c decreases with V_0. Based on these studies, one can draw two major conclusions: (1) contact resistance for tunneling type contact is *voltage-dependent*. This dependence is especially strong for higher voltages [Fig. 5(b)]; (2) the contact current density profiles depend on the interfacial layer properties and geometry, which may enable controlled current transport by *interface engineering*. This will be discussed more in Sec. VI later.

V. 2D-MATERIAL-BASED SCHOTTKY CONTACTS

Schottky contacts based on novel 2D materials, like MoS_2, black phosphorus, and graphene, can be modeled by coupling the thermionic charge injection model for 2D materials[106] with 2D-TLM.[102–104] This self-consistent model accounts for varying specific contact resistivity along the contact length; therefore, it is capable of including the effects of nonuniform doping and interface roughness. The total contact resistance and the current distribution were calculated for electrical contacts between 2D materials and three-dimensional (3D) metals, or between different 2D materials.[104] Results were validated with recent experiments.[66,97,120] The self-consistent model was found to be more accurate than the existing 1D models, especially for small Schottky barrier height (SBH) or large bias voltage.[104]

Roughness engineering was proposed to reduce the large contact resistance at the 3D/2D electrical contacts. Interface roughness is naturally present in the contact area due to defects introduced during the fabrication process. It can also be artificially added, for example, by engineered doping of the substrate.[121] The impact of surface roughness on contact resistance has been studied extensively for ohmic contacts.[60,122–124] In Ref. 104. interface roughness at the 2D/3D electrical contacts is modeled as fluctuating SBHs[125] along the contact length [Fig. 6(a)]. The fluctuation was assumed to follow a Gaussian distribution. Figures 6(b) and 6(c) show the injection current density and the contact resistivity profiles, respectively, for the interface roughness shown in Fig. 6(a).[104] It was found that R_c decreases significantly in the presence of interface roughness and this decrease is more prominent for larger mean SBHs (e.g., 0.3 eV).

The authors of Ref. 104 suggested that roughness reduces the contact resistance in 2D-material-based contacts with 3D metals, enabling a new viable route toward the design of better electrical contacts to 2D materials using roughness engineering.[104]

VI. INTERFACE ENGINEERING OF ELECTRICAL CONTACTS

Over the years, several efforts have been made to reduce the current crowding and improve the current transport in electrical contacts. State-of-the-art methods include proper choice for electrode thickness,[126] doping, electrode material and its geometry;[127–129] optimization of the current spreading layer[130] and the gate bias voltage;[65] reduction of the injection barrier at the contact interface with thin interlayers; and insertion of additional control contacts to increase charge injection.[131] These suggestions require either extra interfacial layers, or particularly chosen material combination and electrode properties. An alternative approach[107] was suggested that deals with the problem locally and may not require an additional material or component.

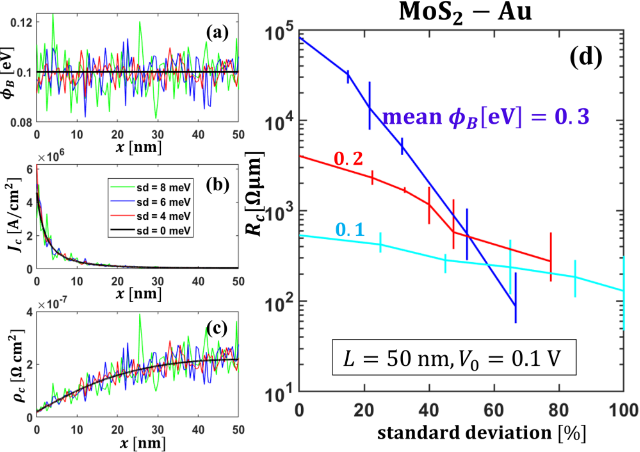

FIG. 6. (a) Roughness in Schottky barrier height ϕ_B, the resulting (b) current density $J_c(x)$, and (c) specific contact resistivity $\rho_c(x)$ across the contact interface for a monolayer MoS_2-Au 2D/3D contact for different standard deviations (sd) of the SBHs. (d) Contact resistance R_c as a function of surface roughness (standard deviation/ϕ_B) for different mean values of ϕ_B. Here, applied voltage $V_0 = 0.1$ V, and contact length $L = 50$ nm. Reprinted with permission from Banerjee *et al.*, Phys. Rev. Appl. **13**, 064021 (2020). Copyright 2020 American Physical Society.

Published under an exclusive license by the AVS

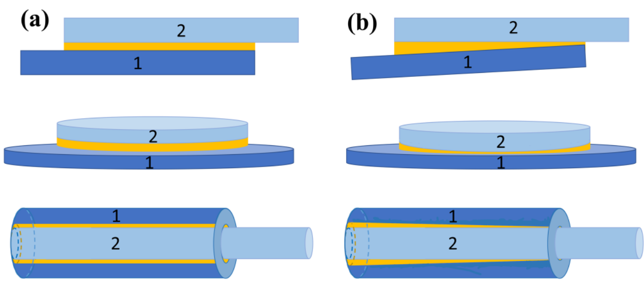

FIG. 7. Electrical contact between contact members 1 and 2 for different electrode geometry. (a) Electrical contacts with uniform contact interface, (b) electrical contacts with a spatially varying engineered interfacial layer, which is used to control the voltage and current distribution. Reprinted with permission from Banerjee *et al.*, Phys. Rev. Appl. **15**, 064048 (2021). Copyright 2021 American Physical Society.

By varying the interfacial layer properties and geometry, the current and voltage profiles across the contact area can be precisely customized.[105,107] The lumped circuit TLM equations (Sec. IV)[102,103] coupled with the quantum tunneling model for MIM junctions (Sec. III),[84] or the thermionic emission current injection model for 2D materials were solved self-consistently to obtain the current and voltage profiles.[104,106] The proposed interface engineering method relies on strategical variation of the specific contact resistivity ρ_c along the contact length. The spatial variation of ρ_c may be achieved by varying the doping, thickness (Fig. 7), or shape of the contact layer, or by introducing impurities along the contact length. Figure 4 shows that high ρ_c reduces current crowding but increases the overall contact resistance R_c.

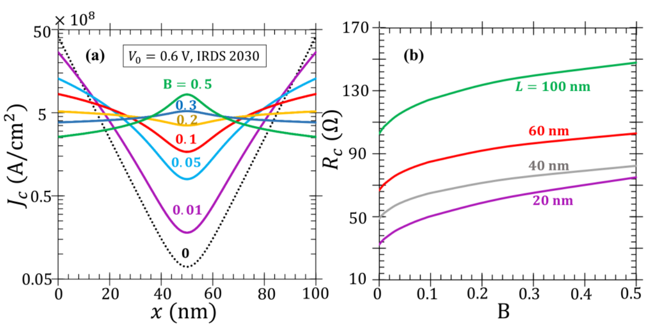

FIG. 8. Engineered Cu/Cu ohmic contact in a Cartesian geometry with specific contact resistivity $\rho_c(x) = 18 \times 10^{-10}(B\,(2x/L - 1)^2 + 0.01)\,\Omega\,\text{cm}^2$. (a) Contact current density $J_c(x)$ along the contact length for different values of B; (b) contact resistance as a function of B for different contact length L. The input voltage $V_0 = 0.6\,\text{V}$ is the required industry standards according to the International Roadmap of Devices and Systems (IRDS) (Ref. 132) for year 2030. The thickness of both Cu contact members is 10 nm, with a resistivity of $18\,\mu\Omega\,\text{cm}$ (Ref. 133), which gives sheet resistance $R_{sh1} = R_{sh2} = 18\,\Omega/\square$. Contact length $L = 100\,\text{nm}$ in (a), and the width (transverse dimension) of the contact members $w = 10\,\text{nm}$. Reprinted with permission from Banerjee *et al.*, Phys. Rev. Appl. **15**, 064048 (2021). Copyright 2021 American Physical Society.

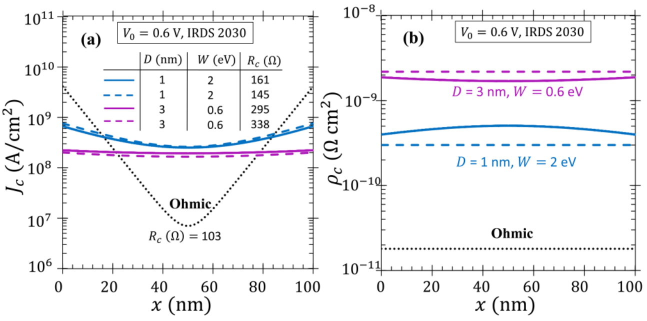

FIG. 9. Tunneling contact engineering. (a) Contact current density $J_c(x)$, and (b) specific contact resistivity $\rho_c(x)$ along the contact length for Cartesian tunneling contacts. Solid lines are for self-consistent numerical calculations with MIM quantum tunneling formulations (Sec. III) (Refs. 21 and 84) for different values of gap distance D and work function of contact members W. Sheet resistance of both the contact members is assumed to be $R_{sh1} = R_{sh2} = 18\,\Omega/\square$. Dashed lines are calculated analytically with constant ρ_c using $V_g = V_0$ in the 1D MIM tunneling model. Black dotted lines are for an ohmic contact with $\rho_c = 1.8 \times 10^{-11}\,\Omega\,\text{cm}^2$, analytically calculated from the TLM equations. R_c is the total contact resistance. Reprinted with permission from Banerjee *et al.*, Phys. Rev. Appl. **15**, 064048 (2021). Copyright 2021 American Physical Society.

Thus, the main challenge is to reduce the current crowding effect without degrading the total current transport considerably.

It was found that the severe current crowding at the highly conductive planar Cu/Cu ohmic contacts can be reduced by varying the specific contact resistivity parabolically along the contact length.[107] As exemplified in Fig. 8, it is possible to achieve approximately uniform contact current distribution without increasing the total contact resistance significantly. The main idea is to make the contact interface more resistive near the contact edges and less resistive in the center region. Current crowding can also be reduced by varying $\rho_c(x)$ as a simple step function along x, which is expected to be easier to implement in practice.[107]

Motivated by the nonlinear J–V characteristics of tunneling junctions (Sec. III), *tunneling contact engineering* was also proposed to effectively eliminate current crowding in highly conductive ohmic contacts, in which a thin (in nm or sub-nm) tunneling layer of thickness (D) was introduced between the contact members. The profiles of contact current density J_c with different tunneling layer thickness and contact member work function were exemplified in Fig. 9 (Ref. 107). The distribution of J_c across the contact area is much more uniform for contacts with a tunneling layer [colored lines in Fig. 9(a)]. Although ρ_c increases significantly when a tunneling gap is introduced, as shown in Fig. 9(b), the total contact resistance R_c is still kept on the same order, as seen in the inset table of Fig. 9(a).

VII. CONCLUSION

Motivated by the challenges of physical scaling down of electrical circuits, the growing demands for low-dimensional material-based devices, and the need for improved controllability of the current transport at the interfaces, this paper attempts to collate

Published under an exclusive license by the AVS

recent studies on modeling of nanoscale electrical junctions and electrical contacts.[18] First, a generalized self-consistent model for quantum tunneling in MIM nanojunctions[21,84] was discussed. The rectification property of dissimilar electrode MIM junction was studied for different material properties and input parameters. Then, recent studies on current distribution and contact resistance in nanoscale electrical contacts were presented. The recently proposed 2D-TLM accounts for the spatial variation of specific contact resistivity.[102,103] With this model, three possible methods of improving electrical contacts and mitigate current crowding were studied: (1) *roughness engineering* of 2D-material-based contacts in order to reduce large contact resistance at the 2D/3D interfaces,[104] (2) *interface engineering* of electrical contacts, and (3) *tunneling contact engineering* to reduce current crowding in highly conductive ohmic contacts.[107]

The models for the MIM tunneling junctions did not consider the effects of electrode geometry, insulator layer imperfections (such as charge trapping, impurities inside the insulator, etc.) and AC driven frequency dependence of the tunneling current. These effects may be studied in future works. The application of the model to nanoscale electrical structures with time-varying excitations, such as split-ring resonator arrays and THz-STMs, may also be explored.[4,134] It is also interesting to find the connection of the quantum tunneling models to field emission from ultrathin dielectric coated surfaces[135,136] and optical field driven photoelectron emission in nanoscale gaps.[37,137] Although widely used, both the free-electron gas model and the WKB approximation used in this model need to be carefully examined in the future. One may directly solve the time-independent Schrödinger equation numerically to get a more accurate description of the transmission probability.[138]

The scope of future works on the modeling of current flow distribution and contact resistance at nanoscale electrical contacts remains vast. The effects of more complicated contact geometry,[11,139,140] insulator layer non-uniformities, and the time-dependent response of the electrical contacts need to be investigated. Coupled electrical–thermal transport across nanoscale electrical contacts with the effects of temperature-dependent electrical and/or thermal conductivities[16,55] requires extensive future studies. It is also important to look at the extension of the theory to a contact structure with multiple interfacial layers with anisotropic material properties. Note that, although widely used, TLM is only a simplified approximation of the practical electrical contacts, where the impacts of finite interfacial layer thickness, current crowding and fringing fields near the contact corners cannot be fully accounted for.[9,65,94] In the future, field solution methods[9,47,94,139] need to be incorporated to accurately quantify these effects. The regimes in which TLM becomes invalid need to be carefully determined in the future.

ACKNOWLEDGMENTS

This work was supported by the Air Force Office of Scientific Research (AFOSR) YIP Grant (No. FA9550-18-1-0061) and Sandia's 01355 Electrical Models and Simulation group. Sandia National Laboratories is a multimission laboratory managed and operated by the National Technology and Engineering Solutions of Sandia, LLC, a wholly owned subsidiary of Honeywell International Inc., for the U.S. Department of Energy's National Nuclear Security Administration under Contract No. DE-NA0003525. This paper describes objective technical results and analysis. Any subjective views or opinions that might be expressed in the paper do not necessarily represent the views of the U.S. Department of Energy or the United States Government.

AUTHOR DECLARATIONS

Conflict of Interest

The authors have no conflicts to disclose.

DATA AVAILABILITY

The data that support the findings of this study are available from the corresponding author upon reasonable request.

REFERENCES

[1] M. Ieong, B. Doris, J. Kedzierski, K. Rim, and M. Yang, Science **306**, 2057 (2004).
[2] J. Zheng *et al.*, Sci. Rep. **3**, 1314 (2013).
[3] Tersoff and S. B. Hamann, Phys. Rev. B: Condens. Matter **31**, 805 (1985).
[4] T. L. Cocker *et al.*, Nat. Photonics **7**, 620 (2013).
[5] D. K. Schroder, *Semiconductor Material and Device Characterization* (Wiley-Blackwell, Hoboken, New Jersey, 1998).
[6] *Electrical Contacts: Principles and Applications*, 2nd ed., edited by Paul G. Slade (CRC, Boca Raton, 2017).
[7] P. Zhang, Y. Y. Lau, and R. M. Gilgenbach, J. Appl. Phys. **109**, 124910 (2011).
[8] P. Zhang, Y. Y. Lau, and R. S. Timsit, IEEE Trans. Electron Devices **59**, 1936 (2012).
[9] P. Zhang, Y. Y. Lau, and R. M. Gilgenbach, J. Phys. D: Appl. Phys. **48**, 475501 (2015).
[10] M. A. Mackey, M. R. K. Ali, L. A. Austin, R. D. Near, and M. A. El-Sayed, J. Phys. Chem. B **118**, 1319 (2014).
[11] P. Zhang, Q. Gu, Y. Y. Lau, and Y. Fainman, IEEE J. Quantum Electron. **52**, 2000207 (2016).
[12] M. S. Ghamsari and S. Dhara, *Nanorods and Nanocomposites* (London, United Kingdom, IntechOpen, 2020).
[13] S. E. Wawra, L. Pflug, T. Thajudeen, C. Kryschi, M. Stingl, and W. Peukert, Nat. Commun. **9**, 1 (2018).
[14] N. Behabtu *et al.*, Science **339**, 182 (2013).
[15] P. Zhang, S. B. Fairchild, T. C. Back, and Y. Luo, AIP Adv. **7**, 125203 (2017).
[16] P. Zhang, J. Park, S. B. Fairchild, N. P. Lockwood, Y. Y. Lau, J. Ferguson, and T. Back, Appl. Sci. **8**, 1175 (2018).
[17] S. B. Fairchild, P. Zhang, J. Park, T. C. Back, D. Marincel, Z. Huang, and M. Pasquali, IEEE Trans. Plasma Sci. **47**, 2032 (2019).
[18] S. Banerjee, "Modeling of nanoscale electrical junctions and electrical contacts," Ph.D. thesis (Michigan State University, 2021).
[19] J. G. Simmons, J. Appl. Phys. **34**, 1793 (1963).
[20] C. Li, E. T. Thostenson, and T.-W. Chou, Appl. Phys. Lett. **91**, 223114 (2007).
[21] P. Zhang, Sci. Rep. **5**, 9826 (2015).
[22] See https://semiengineering.com/making-chips-at-3nm-and-beyond/ for "Making Chips at 3 nm and Beyond," Semiconductor Engineering, 16 April 2020.
[23] See https://www.anandtech.com/show/16024/tsmc-details-3nm-process-technology-details-full-node-scaling-for-2h22 for "TSMC Details 3 nm Process Technology: Full Node Scaling for 2H22 Volume Production."
[24] I. Gayduchenko *et al.*, Nat. Commun. **12**, 543 (2021).
[25] A. Seabaugh, "The Tunneling Transistor," *IEEE Spectrum: Technology, Engineering, and Science News*, September 30, 2013; available at https://spectrum.ieee.org/semiconductors/devices/the-tunneling-transistor

Published under an exclusive license by the AVS

[26]T. Ihn *et al.*, Mater. Today **13**, 44 (2010).
[27]C. Thelander, T. Mårtensson, M. T. Björk, B. J. Ohlsson, M. W. Larsson, L. R. Wallenberg, and L. Samuelson, Appl. Phys. Lett. **83**, 2052 (2003).
[28]H. W. C. Postma, T. Teepen, Z. Yao, M. Grifoni, and C. Dekker, Science **293**, 76 (2001).
[29]R. Patel, Y. Agrawal, and R. Parekh, Microsyst. Technol. **27**, 1863 (2020).
[30]P. Zhang and Y. Y. Lau, J. Plasma Phys. **82**, 595820505 (2016).
[31]S. Srisonphan, Y. S. Jung, and H. K. Kim, Nat. Nanotechnol. **7**, 504 (2012).
[32]P. Zhang, A. Valfells, L. K. Ang, J. W. Luginsland, and Y. Y. Lau, Appl. Phys. Rev. **4**, 011304 (2017).
[33]B. R. Stoner and J. T. Glass, Nat. Nanotechnol. **7**, 485 (2012).
[34]G. Wu, X. Wei, S. Gao, Q. Chen, and L. Peng, Nat. Commun. **7**, 11513 (2016).
[35]See https://spectrum.ieee.org/semiconductors/devices/introducing-the-vacuum-transistor-a-device-made-of-nothing for "Introducing the Vacuum Transistor: A Device Made of Nothing - IEEE Spectrum," IEEE Spectrum: Technology, Engineering, and Science News.
[36]J. Lin, P. Y. Wong, P. Yang, Y. Y. Lau, W. Tang, and P. Zhang, J. Appl. Phys. **121**, 244301 (2017).
[37]Y. Luo and P. Zhang, Appl. Phys. Lett. **119**, 194101 (2021).
[38]P. Zhang, Y. S. Ang, A. L. Garner, A. Valfells, J. W. Luginsland, and L. K. Ang, J. Appl. Phys. **129**, 100902 (2021).
[39]G. Aguirregabiria, D. C. Marinica, R. Esteban, A. K. Kazansky, J. Aizpurua, and A. G. Borisov, Phys. Rev. B **97**, 115430 (2018).
[40]J.-W. Han, J. Sub Oh, and M. Meyyappan, Appl. Phys. Lett. **100**, 213505 (2012).
[41]J.-W. Han, D.-I. Moon, and M. Meyyappan, Nano Lett. **17**, 2146 (2017).
[42]J. Yoon, M. Lim, B. Choi, D. M. Kim, D. H. Kim, S. Kim, and S.-J. Choi, Sci. Rep. **7**, 5453 (2017).
[43]B. E. Kilbride, J. N. Coleman, J. Fraysse, P. Fournet, M. Cadek, A. Drury, S. Hutzler, S. Roth, and W. J. Blau, J. Appl. Phys. **92**, 4024 (2002).
[44]M. Foygel, R. D. Morris, D. Anez, S. French, and V. L. Sobolev, Phys. Rev. B **71**, 104201 (2005).
[45]J. Tang, Q. Cao, G. Tulevski, K. A. Jenkins, L. Nela, D. B. Farmer, and S.-J. Han, Nat. Electron. **1**, 191 (2018).
[46]L.-M. Peng, Nat. Electron. **1**, 158 (2018).
[47]P. Zhang, D. M. H. Hung, and Y. Y. Lau, J. Phys. D: Appl. Phys. **46**, 065502 (2013).
[48]P. Zhang, Y. Y. Lau, and R. M. Gilgenbach, Appl. Phys. Lett. **97**, 204103 (2010).
[49]H. Murrmann and D. Widmann, IEEE Trans. Electron Devices **16**, 1022 (1969).
[50]P. Zhang and Y. Y. Lau, IEEE J. Electron Devices Soc. **1**, 83 (2013).
[51]R. Holm, *Electric Contacts: Theory and Application*, 4th ed. (Springer-Verlag, Berlin Heidelberg, 1967).
[52]R. S. Timsit, IEEE Trans. Compon. Packaging Technol. **22**, 85 (1999).
[53]A. M. Rosenfeld and R. S. Timsit, Q. Appl. Math. **39**, 405 (1981).
[54]R. S. Timsit, in *Encyclopedia of Tribology*, edited by Q. J. Wang and Y.-W. Chung (Springer US, Boston, MA, 2013), p. 903.
[55]F. Antoulinakis, D. Chernin, P. Zhang, and Y. Y. Lau, J. Appl. Phys. **120**, 135105 (2016).
[56]M. Pedram, ACM Trans. Des. Autom. Electron. Syst. **1**, 3 (1996).
[57]M. Pedram and S. Nazarian, Proc. IEEE **94**, 1487 (2006).
[58]Review of federal programs for wire system safety National Science and Technology Council Final Report.
[59]J. S. Kuzniar and G. A. Slenski, "Wire integrity field survey of USAF legacy aircraft ReportADP014075, 2001."
[60]P. Zhang, "Effects of surface roughness on electrical contact, RF heating and field enhancement," Ph.D. thesis (University of Michigan, 2012).
[61]K. N. Tu, Y. Liu, and M. Li, Appl. Phys. Rev. **4**, 011101 (2017).
[62]M. R. Gomez, J. C. Zier, R. M. Gilgenbach, D. M. French, W. Tang, and Y. Y. Lau, Rev. Sci. Instrum. **79**, 093512 (2008).
[63]M. Park, B. A. Cola, T. Siegmund, J. Xu, M. R. Maschmann, T. S. Fisher, and H. Kim, Nanotechnology **17**, 2294 (2006).
[64]F. Antoulinakis and Y. Y. Lau, J. Appl. Phys. **127**, 125107 (2020).
[65]Q. Wang, X. Tao, L. Yang, and Y. Gu, Appl. Phys. Lett. **108**, 103109 (2016).
[66]Y. Wang *et al.*, Nature **568**, 70 (2019).
[67]K. L. Grosse, M.-H. Bae, F. Lian, E. Pop, and W. P. King, Nat. Nanotechnol. **6**, 287 (2011).
[68]P. Karnatak, T. P. Sai, S. Goswami, S. Ghatak, S. Kaushal, and A. Ghosh, Nat. Commun. **7**, 13703 (2016).
[69]M. D. Haworth *et al.*, IEEE Trans. Plasma Sci. **26**, 312 (1998).
[70]E. Schrödinger, Phys. Rev. **28**, 1049 (1926).
[71]H. A. Kramers, Z. Phys. **39**, 828 (1926).
[72]G. Wentzel, Z. Phys. **38**, 518 (1926).
[73]A. Sommerfield and H. Bethe, *Handbuch der Physik* (Springer-Verlag, Berlin, 1933).
[74]R. Holm and B. Kirschstein, Z. Tech. Physik **16**, 488 (1935).
[75]J. G. Simmons, J. Appl. Phys. **34**, 2581 (1963).
[76]V. D. Das and M. S. Jagadeesh, Phys. Status Solidi (A) **66**, 327 (1981).
[77]Y. Y. Lau, D. Chernin, D. G. Colombant, and P.-T. Ho, Phys. Rev. Lett. **66**, 1446 (1991).
[78]L. K. Ang, T. J. T. Kwan, and Y. Y. Lau, Phys. Rev. Lett. **91**, 208303 (2003).
[79]L. K. Ang and P. Zhang, Phys. Rev. Lett. **98**, 164802 (2007).
[80]S. Bhattacharjee and T. Chowdhury, Appl. Phys. Lett. **95**, 061501 (2009).
[81]S. Bhattacharjee, A. Vartak, and V. Mukherjee, Appl. Phys. Lett. **92**, 191503 (2008).
[82]L. K. Ang, Y. Y. Lau, and T. J. T. Kwan, IEEE Trans. Plasma Sci. **32**, 410 (2004).
[83]R. H. Fowler and L. Nordheim, Proc. R. Soc. London A **119**, 173 (1928).
[84]S. Banerjee and P. Zhang, AIP Adv. **9**, 085302 (2019).
[85]P. M. Hall, Thin Solid Films **1**, 277 (1968).
[86]P. M. Hall, Thin Solid Films **300**, 256 (1997).
[87]M. W. Denhoff, J. Phys. D: Appl. Phys. **39**, 1761 (2006).
[88]D. P. Kennedy and P. C. Murley, IBM J. Res. Dev. **12**, 242 (1968).
[89]H. H. Berger, J. Electrochem. Soc. **119**, 507 (1972).
[90]G. K. Reeves, Solid-State Electron. **23**, 487 (1980).
[91]G. K. Reeves and B. Harrison, IEEE Trans. Electron Devices **42**, 1536 (1995).
[92]G. K. Reeves, P. W. Leech, and H. B. Harrison, Solid-State Electron. **38**, 745 (1995).
[93]G. K. Reeves and H. B. Harrison, Solid-State Electron. **41**, 1067 (1997).
[94]P. Zhang and Y. Y. Lau, Appl. Phys. Lett. **104**, 204102 (2014).
[95]E. G. Woelk, H. Krautle, and H. Beneking, IEEE Trans. Electron Devices **33**, 19 (1986).
[96]C. Lan, P. Srisungsitthisunti, P. B. Amama, T. S. Fisher, X. Xu, and R. G. Reifenberger, Nanotechnology **19**, 125703 (2008).
[97]C. D. English, G. Shine, V. E. Dorgan, K. C. Saraswat, and E. Pop, Nano Lett. **16**, 3824 (2016).
[98]D. Somvanshi, S. Kallatt, C. Venkatesh, S. Nair, G. Gupta, J. K. Anthony, D. Karmakar, and K. Majumdar, Phys. Rev. B **96**, 205423 (2017).
[99]J. S. Moon *et al.*, Appl. Phys. Lett. **100**, 203512 (2012).
[100]R. Piotrzkowski, E. Litwin-Staszewska, and Sz. Grzanka, Appl. Phys. Lett. **99**, 052101 (2011).
[101]K. He, Y. Li, X. Chen, H. Hua, Y.-L. Gao, Z.-H. Ye, C. Lin, J.-X. Wang, and Q.-Y. Zhang, J. Appl. Phys. **115**, 164506 (2014).
[102]S. Banerjee, J. Luginsland, and P. Zhang, Sci. Rep. **9**, 14484 (2019).
[103]S. Banerjee, P. Y. Wong, and P. Zhang, J. Phys. D: Appl. Phys. **53**, 355301 (2020).
[104]S. Banerjee, L. Cao, Y. S. Ang, L. K. Ang, and P. Zhang, Phys. Rev. Appl. **13**, 064021 (2020).
[105]P. Zhang, S. Banerjee, and J. Luginsland, U.S. patent 10,755,975 B2 (25 August 2020).

Published under an exclusive license by the AVS

[106]Y. S. Ang, H. Y. Yang, and L. K. Ang, Phys. Rev. Lett. **121**, 056802 (2018).
[107]S. Banerjee, J. Luginsland, and P. Zhang, Phys. Rev. Appl. **15**, 064048 (2021).
[108]A. Singh, "Improving current-asymmetry of metal-insulator-metal tunnel junctions," Electronic Theses and Dissertations (FIU, October 2016).
[109]S. Krishnan, S. Bhansali, E. Stefanakos, and Y. Goswami, Proc. Chem. **1**, 409 (2009).
[110]K. Choi, F. Yesilkoy, G. Ryu, S. H. Cho, N. Goldsman, M. Dagenais, and M. Peckerar, IEEE Trans. Electron Devices **58**, 3519 (2011).
[111]L. Wu, H. Duan, P. Bai, M. Bosman, J. K. W. Yang, and E. Li, ACS Nano **7**, 707 (2013).
[112]J. P. Perdew and Y. Wang, Phys. Rev. B **45**, 13244 (1992).
[113]M. A. Omar, *Elementary Solid State Physics: Principles and Applications* (Boston, MA, 2016).
[114]D. Bohm, *Quantum Theory* (Prentice-Hall, New York, 1951).
[115]P. Février and J. Gabelli, Nat. Commun. **9**, 4940 (2018).
[116]M. Uiberacker *et al.*, Nature **446**, 627 (2007).
[117]G. Nimtz, Found. Phys. **41**, 1193 (2011).
[118]K. K. Thornber, T. C. McGill, and C. A. Mead, J. Appl. Phys. **38**, 2384 (1967).
[119]K. L. Jensen, A. Shabaev, J. Riga, D. A. Shiffler, J. L. Lebowitz, and R. Seviour, Phys. Rev. A **104**, 062203 (2021).
[120]K. K. H. Smithe, C. D. English, S. V. Suryavanshi, and E. Pop, 2D Mater. **4**, 011009 (2016).
[121]N. Kaushik, A. Nipane, F. Basheer, S. Dubey, S. Grover, M. M. Deshmukh, and S. Lodha, Appl. Phys. Lett. **105**, 113505 (2014).
[122]F. Pennec, D. Peyrou, D. Leray, P. Pons, R. Plana, and F. Courtade, IEEE Trans. Compon. Packaging Technol. **2**, 85 (2012).
[123]Z. A. Lamport *et al.*, Nat. Commun. **9**, 5130 (2018).
[124]Y. Gao, L. Liu, W. Ta, and J. Song, AIP Adv. **8**, 035319 (2018).
[125]S.-J. Liang, W. Hu, A. Di Bartolomeo, S. Adam, and L. K. Ang, *2016 IEEE International Electron Devices Meeting (IEDM) San Francisco, CA, 3–7 Dec. 2016* (IEEE, 2016).
[126]C.-K. Wang, T.-H. Chiang, Y.-Z. Chiou, and S.-P. Chang, Jpn. J. Appl. Phys. **52**, 01AG05 (2013).
[127]G. Kim, J. H. Kim, E. Park, and B.-G. Park, J. Semicond. Technol. Sci. **14**, 558 (2014).
[128]N. Shamir and D. Ritter, Solid-State Electron. **47**, 127 (2003).
[129]S.-S. Chee *et al.*, Adv. Mater. **31**, 1804422 (2019).
[130]Y. Zhang, M. Sun, D. Piedra, J. Hennig, A. Dadgar, and T. Palacios, Appl. Phys. Lett. **111**, 163506 (2017).
[131]F. Torricelli, L. Colalongo, D. Raiteri, Z. M. Kovács-Vajna, and E. Cantatore, Nat. Commun. **7**, 10550 (2016).
[132]See https://irds.ieee.org/editions/2017 for International Roadmap for Devices and Systems (IRDSTM) 2017.
[133]E. Schmiedl, P. Wissmann, and H.-U. Finzel, Z. Naturforsch. A **63**, 739 (2014).
[134]K. Yoshioka, I. Katayama, Y. Minami, M. Kitajima, S. Yoshida, H. Shigekawa, and J. Takeda, Nat. Photonics **10**, 762 (2016).
[135]X. Xiong, Y. Zhou, Y. Luo, X. Li, M. Bosman, L. K. Ang, P. Zhang, and L. Wu, ACS Nano **14**, 8806 (2020).
[136]Y. Zhou and P. Zhang, Phys. Rev. Res. **2**, 043439 (2020).
[137]Y. Luo and P. Zhang, Phys. Rev. Appl. **17**, 044008 (2022).
[138]K. L. Jensen, *Introduction to the Physics of Electron Emission*, 1st ed. (Wiley, Hoboken, NJ, 2017).
[139]P. Yang, S. Banerjee, W. Kuang, Y. Ding, Q. Ma, and P. Zhang, J. Phys. D: Appl. Phys. **53**, 485303 (2020).
[140]P. Zhang and D. M. H. Hung, J. Appl. Phys. **115**, 204908 (2014).

Sneha Banerjee received the B.S. degree in Electronics and Communication Engineering from West Bengal University of Technology, India, in 2012 and the M.S. degree in Radio Physics and Electronics from the University of Calcutta, India, in 2015. She received her Ph. D. degree in Electrical and Computer Engineering from Michigan State University in 2021. She is working at Sandia National Laboratories as a postdoc. Her current research interests include quantum tunneling, semiconductor device simulation, electron emission, and contact engineering. She is a recipient of Michigan Institute of Plasma Science and Engineering (MIPSE) Graduate Fellowship Award in 2020–2021, the 2020 MIPSE Graduate Student Symposium Best Presentation Award, the 2020–2021 Michigan State University Electrical Engineering Outstanding Graduate Student Award, and the 2021 IEEE Nuclear and Plasma Sciences Society (NPSS) Graduate Scholarship Award. Sneha was also the Founder of IEEE NPSS Student Chapter at Michigan State University (Feb 2020) and served as the President from 2020 to 2021.

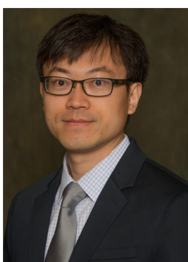

Peng Zhang received the B.Eng. and M.Eng. degrees in electrical and electronic engineering from Nanyang Technological University, Singapore, in 2006 and 2008, respectively, and the Ph.D. degree in nuclear engineering and radiological sciences from the University of Michigan (UM), Ann Arbor, MI, USA, in 2012. He was an Assistant Research Scientist at UM (2013–2016). He is currently an Associate Professor (Assistant Professor, 2016–2021) with the Department of Electrical and Computer Engineering, Michigan State University (MSU), East Lansing, MI, USA. He has authored or co-authored 96 refereed journal articles on electrical contacts, classical, ballistic, and quantum diodes, space-charge-limited beams, multipactor and breakdown, rf heating, z-pinches, laser–plasma interaction, ultrafast photoemission, and novel radiation sources. His current research interests include theoretical and computational physics in nanoelectronics, plasmas, and accelerator technology. Dr. Zhang is currently serving as an Editorial Board Member for Scientific Reports and Plasma Research Express. He was a Guest Editor of the 2020 Special Issue of the IEEE Transactions on Plasma Science on High-Power Microwave and Millimeter Wave Generation. He served as a member of the IEEE Plasma Science and Application (PSAC) Executive Committee (2018–2021). He was a recipient of the IEEE Nuclear and Plasma Sciences Society (NPSS) Early Achievement Award (2020), the Office of Naval Research (ONR) Young Investigator Program Award (2020), the Air Force Office of Scientific Research (AFOSR) Young Investigator Program Award (2018), the UM Rackham Presidential Fellowship Award (2011), and the UM Richard and Eleanor Towner Prize for Outstanding Ph.D. Research (2010).

Published under an exclusive license by the AVS